

Flow characteristics after water inrush from the working face in karst tunneling

J. Wu^a, S.C. Li^b, Z.H. Xu^{*}, D.D. Pan^c and S.J. He^d

Geotechnical and Structural Engineering Research Center, Shandong University, Ji'nan 250061, Shandong, China

(Received January 27, 2017, Revised May 30, 2017, Accepted September 3, 2017)

Abstract. In order to investigate flow characteristics after water inrush from the working face in process of karst tunnel construction, numerical calculation for two class case studies of water inrush is carried out by using the FLUENT software on the background of Qiyueshan tunnel. For each class water inrush from the tunnel face, five cases under different water-inrush velocity are simulated and researched. Three probing lines are selected respectively in the left tunnel, cross passage, right tunnel and in the height direction of the tunnel centerline. The variation characteristics of velocity and pressure on each probing line under the five water-inrush velocities are analyzed. As for the selected four groups probing lines in the tunnels, the change rules of velocity and pressure on each group probing lines under the same water-inrush velocity are discussed. Finally, the water flow characteristics after inrush from the tunnel face are summarized by comparing the case studies. The results indicate that: (1) The velocity and pressure change greatly at the intersection area of the cross passage and the tunnels. (2) The velocity nearby the tunnel side wall is the minimum, while it is the maximum in the middle position. (3) The pressure value of every cross section in the tunnels is basically fixed. (4) As water-inrush velocity increases, the flow velocity and pressure in the tunnels also increase. The former is approximately proportional to their respective water-inrush velocity, while the latter is not. The research results provide a theoretical basis for making scientific and rational escape routes.

Keywords: karst tunnel; tunnel face; water inrush; velocity and pressure; flow characteristics

1. Introduction

Large-scale construction of deep and long tunnels greatly promotes the development of tunnel construction technology. In the 21st century, a large number of railway and highway traffic engineering, hydroelectric engineering and other major foundation engineering have been put on Chinese transport, hydro-power and other fields, besides, more than 10,000 kilometers railway and highway tunnels have been built (Wei *et al.* 2010, Meng *et al.* 2012, Khezri *et al.* 2016).

With the development of transport and hydro-power engineering construction, the focus is shifting to karst area and western mountains of China with extremely complex geological condition (Hu *et al.* 2008, Huang *et al.* 2010, Zhou *et al.* 2015). Ten thousand kilometers tunnel projects and twenty world-class large hydropower projects are being planned or constructed. There will be an array of high risk karst tunnel engineering, which has remarkable characteristics of great depth, long tunnel line, high stress,

strong karst, high water pressure, complex geological structures and disaster-prone. In high risk karst areas, water inrush affected by landform, geological structure, formation lithology and other factors often happens in the course of construction, which brings great difficulties to tunneling (Islam and Islam 2005, Ma *et al.* 2010, Divall and Goodey 2015).

Now, water inrush has become the most common geological disaster during the construction and operation of tunnels, mines and other underground engineering (Golob *et al.* 1998, Wang *et al.* 2012, Li *et al.* 2016). As far as concerned the disaster sources, karst is one of the major disaster sources of water inrush. Large-scale water storage structure is developed in karst region, and a wide range of water flowing channels are also distributed there, meanwhile, karst landform has high porosity and abundant karst water. Therefore, the large water-bearing body, large-scale groundwater recharge network and plentiful water provide favorable occurrence condition for water-inrush disaster sources, which poses a serious threat to tunnel construction (Zhang 2005, Ivars 2006, Rao *et al.* 2016).

Throughout the architectural history of world tunneling and underground engineering, water inrush has been the most serious geological disaster during tunnel construction (Zarei *et al.* 2012, Li and Li 2014). China is one of the countries which suffer most from water inrush in the world. The loss of life and economic losses caused by water and mud inrush are ranked first in all types of geological disasters. According to incomplete statistics, on September 10, 2002, water and mud inrush occurred in Chongqing-Huaihua Railway (Yuanliangshan tunnel), which caused 9 tunnel constructors to die. On January 21, 2006, water

*Corresponding author, Associate Professor

E-mail: zhenhao_xu@sdu.edu.cn

^aPh.D Student

E-mail: wujing9516@163.com

^bProfessor

E-mail: lishucaai@sdu.edu.cn

^cPh.D Student

E-mail: pddyantu@163.com

^dMaster Student

E-mail: hsj686@126.com

Table 1 Typical water inrush accidents during tunnel construction in China since 2000

Tunnel name	Water-inrush type	Occurrence time	Disaster losses
Chongqing-Huaihua Railway (Yuanliangshan tunnel)	Seepage instability of filling-type disaster-causing structure	2001-2004	It appeared 71 times severe water inrush. 9 tunnel constructors died. The maximum water pressure was 4.6 MPa. The maximum water inflow was 72000 m ³ /h.
Yichang-Wanzhou Railway (Maluqing tunnel)	Filling-type cavity and water resisting rock mass	2004-2008	It appeared 19 times severe water inrush. Two large water-inrush disasters of January 21, 2006 and April 11, 2008 made 15 people die. The project was delayed for more than two years.
Yichang-Wanzhou Railway (Yesanguan tunnel)	Filling-type cavity and water resisting rock mass	Aug 5, 2007	Within a half hour, the water inflow and mud inflow respectively up to 151000 m ³ , 53500 m ³ . 10 tunnel constructors died. The project was delayed for six months.
Hurongxi Expressway (Longtan Tunnel)	Seepage instability of fracture zone	2006-2007	It appeared 2 times large-scale mud inrush and 3 times large-scale landslide. Mud inflow exceeded 9000 m ³ . The project was delayed for more than one year.
Ji'an-Lianhua Expressway (Zhongjiashan Tunnel)	Seepage instability of fracture zone	Jul-Aug, 2012	It appeared 14 times water and mud inrush. Water and mud inflow respectively exceeded 20000 m ³ , 27900 m ³ .
Jinping Power Station auxiliary tunnel, conveyance water tunnel	Fracture of water resisting rock mass	August 5, 2007	Water pressure exceeded 10 MPa. The maximum instantaneous water inflow up to 7 m ³ /s. There were many water inrush accidents in construction, which influenced project construction progress seriously.

inrush happened in Yichang-Wanzhou Railway (Maluqing tunnel), which caused 11 deaths. On August 5, 2007, water inrush occurred in Yichang-Wanzhou Railway (Yesanguan tunnel), and 10 tunnel constructors died. Besides, the depth of some tunnels exceeds 2000 m, which has noticeable features of high water pressure, high flow, and high ground stress. For example, Jinping Power Station auxiliary tunnel, conveyance water tunnel, the maximum depth is more than 2500 m. Several water-inrush disasters of high pressure and large flow are encountered in construction. The maximum flow rate and water pressure respectively exceed 7 m³/s, 10 MPa, and the maximum ground stress is close to 70 MPa, which affects construction schedule seriously. More details are listed in Table 1. In addition, water inrush easily induces landslide, surface subsidence, exhaustion of groundwater resources and other series of major secondary disasters in tunnel zone, and causes huge economic losses and negative social impacts.

The earliest research of water inrush focused on the energy field. A large number of casualties caused by major water inrush disaster drew wide attention from the international community. The researches on the conditions of water inrush, failure mode, disaster-causing mechanism, precursor information identification, forecast and early warning have been achieved a series of important results.

Li *et al.* (1996) studied water inrush from the floor by building a structural model of a key stratum based on laminated characteristics of the coal seam floor. The mechanism of water-inrush through the open type of fault was that excessive displacement of key strata between two sides of the fault, took place under the water pressure of the confined aquifer. The reason for water-inrush through the closed type of fault was that the strength failure happens in the key stratum or at the interface between the key stratums in two sides of the fault. Marinelli and Niccoli (2000) presented steady-state analytical solutions for estimating the ground water inflow rate in a mine pit. Wang and Lu (2007) proposed a semi-analytical approach for analyzing the

tunnel water inflow. The approach was developed by using the classical ground water theory. Kong *et al.* (2007) used a theory of seepage instability to estimate the harmfulness of water-inrush from a coal seam floor in a particular coal mine of the Mining Group, Xuzhou. They concluded that as long-wall mining was pushed along, the failure zone was enlarged, the strain increased, and fissures developed correspondingly, resulting in the formation of water-inrush channels. The increase in the water-inrush-index was nearly exponential and the harmfulness of water-inrush in the coal mine increased accordingly. Zhu *et al.* (2008) developed a numerical model of the key strata, which was used to predict failure modes and to help establish rules for safe mining above the aquifer. They concluded that the combined action of mining stress and water pressure ultimately led to water inrush from the floor. Jiang *et al.* (2008) investigated the progressive failure of geological structures and predicted their microseismic activities associated with water inrush. Their studies indicated that it was considerably possible to predict the water inrush using microseismic monitoring with its inherent ability to remotely monitor the progressive failure caused by mining. Li *et al.* (2010) studied the mechanism of water-rock interaction in karst tunnel by using theories of karst geology, engineering hydraulics and fracture mechanics, and explored the effects of such mechanism on water outburst and projecting mud soil during the construction of karst tunnel, meanwhile, the mechanical mechanism of water gushing process was also analyzed. Tang *et al.* (2011) studied the water-inrush mechanism of concealed collapse pillars from the mechanical view. The boundary conditions and strength of water-resistant strata play important roles in influencing water-inrush of collapse pillars. The critical water-inrush pressure was determined by both relative thickness and absolute thickness of water-resistant strata. Yao *et al.* (2012) built numerical models for the roof fracture and seepage development rule by using RFP2D and COMSOL respectively, to analyze the changes in fracture zone, stress, water pressure and seepage vector with the advancement of working face. Shi *et al.* (2014) indicated that both water inrush coefficient and water abundance in aquifers should be taken into consideration when evaluating the danger of water inrush from coal seam floor. They built a prediction model of safe-mining evaluation grade by using the support vector machine, and the results showed that this model had high classification accuracy. More achievements can refer to the publications (Jin *et al.* 2009, Wang and Wang 2011, Zhang *et al.* 2013, Chen *et al.* 2014, Nawel and Salah, 2015, Yang *et al.* 2016).

In conclusion, many studies about occurrence mechanism and control measures of water inrush in karst tunnels have been carried out. Laws of water inrush, calculation of water inflow have formed a relatively perfect scientific system. Comprehensive forecast system of water inrush has also improved gradually. However, conventional investigation often focuses on how to probe and prevent karst water. The investigation for flow characteristics after water inrush is often ignored. The relevant specific study is also seldom involved in the flow characteristics after water inrush from the tunnel face.

In the present study, Qiyueshan high risk karst tunnel is

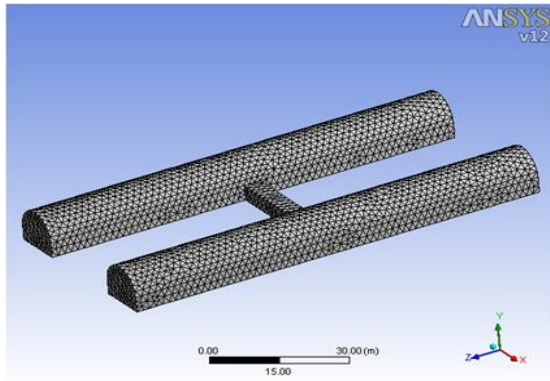


Fig. 1 3D finite element models

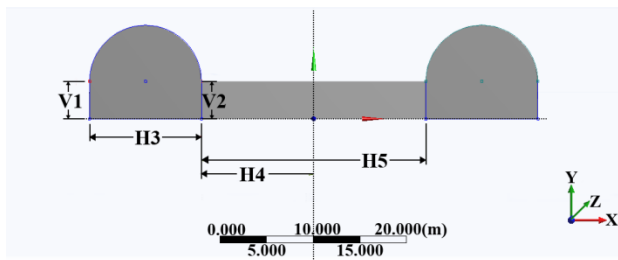


Fig. 2 The model dimensions

Table 2 The parameter setting of the numerical models

Fluid material	20°C liquid water	Gravity	9.8 m/s ²
Density	998.2 kg/m ³	Viscosity	100.3×10 ⁻⁵ pa·s
Thermal conductivity	0.6w/m·k	Specific heat capacity	4182j/kg·k

taken as research background. Computation models and simulated conditions are described in section 2. Numerical calculation for two class case studies of water inrush from the tunnel face is carried out by using FLUENT software. For each class water inrush, five cases with different water-inrush velocity are simulated and researched. For details see sections 3 and 4. Water flow characteristics after inrush from the tunnel face are summarized by comparing these case studies, and some important conclusions are drawn in section 5. The research results can provide a theoretical basis for making optimized escape routes after water inrush. They are also of important guiding significance and engineering value to ensure the safety of tunnel construction.

2. Computation models and simulated conditions

Qiyueshan double-line tunnel is taken as research background, and its section size is adopted. 100 meters behind the working face are chosen for numerical calculation. The 3D finite element models are built, as shown in Fig. 1, and the model dimensions are shown in Fig. 2.

Wherein, V1 and V2 are both equal to 4 m, H3 and H4 are both equal to 12 m, H5 is 24 m. Tunnel cross-sectional area (S) is 104.52 m², the total height of the tunnel (Y) is 10 m (the height of the upper part is 6 m, and the height of the lower part is 4 m), the total length of the tunnel (Z) is 100

m, the distance of axle line between the left tunnel and the right tunnel (X) is 36 m, the width of the cross passage (Z1) is 4 m, the height of the cross passage (Y1) is 4 m, the length of the cross passage (X1) is 24 m, the distance between the axle line of the cross passage and the working face (Z0) is 50 m.

Two class case studies of water inrush from the tunnel face are simulated during the double-line tunnel excavation. The first class case studies, water inrush occurs on the left tunnel working face, and the velocity is 0.1 m/s, 1 m/s, 2 m/s, 3 m/s, 4 m/s, respectively. The left and the right tunnel entrances are both the pressure outlet boundaries. The second class case studies, water inrush occurs on the left tunnel working face (away from the left tunnel entrance), and the velocity is 0.1 m/s, 1 m/s, 2 m/s, 3 m/s, 4 m/s, respectively. But only the right tunnel entrance is the pressure outlet boundary. The left tunnel entrance is the wall boundary.

The standard k-ε turbulence model is a semi-empirical formula. Its computational accuracy, stability and economic performance are all high, which is one of the most widely used turbulence models in engineering flow field calculation. So the standard k-ε turbulence model is adopted in this paper. Suppose the water is incompressible, and the parameter setting of the model is listed in Table 2.

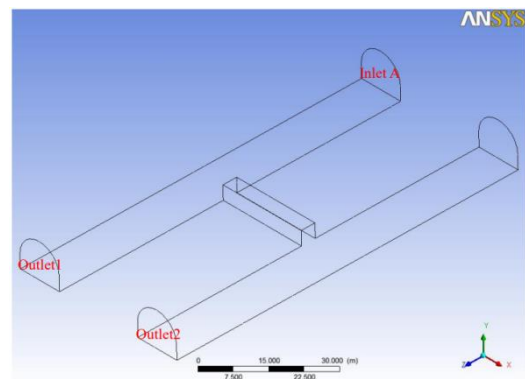


Fig. 3 The water inrush conditions during the double-line tunnel excavation

Table 3 The details of the probing lines

The section	The location	The selected probing lines	The selected points	The figure
Y=2	The left tunnel	N1: X=-14, Y=2, Z=0-100	20	Fig. 4(a)
		N2: X=-18, Y=2, Z=0-100	20	
		N3: X=-22, Y=2, Z=0-100	20	
Y=2	The cross passage	N4: Y=2, Z=48.4, X=-12-12	20	Fig. 4(b)
		N5: Y=2, Z=50.0, X=-12-12	20	
		N6: Y=2, Z=51.6, X=-12-12	20	
Y=2	The right tunnel	N7: X=14, Y=2, Z=0-100	20	Fig. 4(c)
		N8: X=18, Y=2, Z=0-100	20	
		N9: X=22, Y=2, Z=0-100	20	
X=-18	The left tunnel	N10: X=-18, Y=0.4, Z=0-50	10	Fig. 4(d)
		N11: X=-18, Y=2.0, Z=0-50	10	
		N12: X=-18, Y=3.6, Z=0-50	10	

Table 3 Continued

The section	The location	The selected probing lines	The selected points	The figure
Z=50	The cross passage	N10: Y=0.4, Z=50, X=-18-18	10	
		N11: Y=2.0, Z=50, X=-18-18	10	
		N12: Y=3.6, Z=50, X=-18-18	10	
X=18	The right tunnel	N10: X=18, Y=0.4, Z=50-100	10	
		N11: X=18, Y=2.0, Z=50-100	10	
		N12: X=18, Y=3.6, Z=50-100	10	

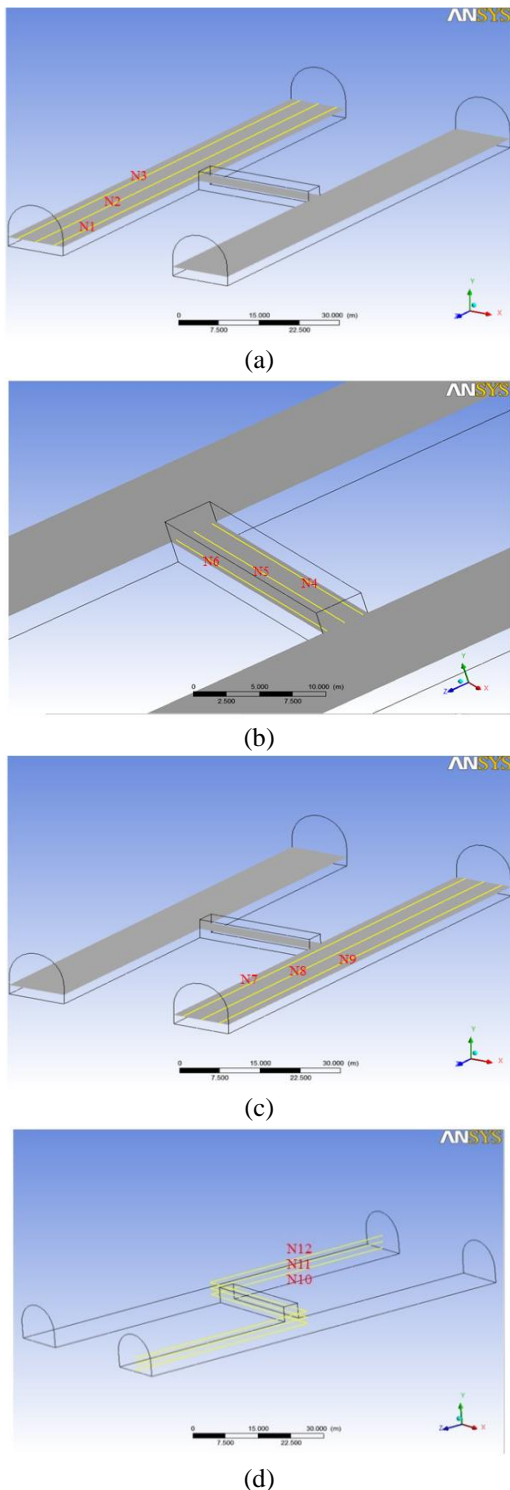


Fig. 4 The locations of the probing lines

3. The first class case studies

Take as an example the most common water inrush in the actual tunnel works. During the double-line tunnel excavation, water inrush occurs on the left tunnel working face, thus, the left tunnel working face is the inlet of water inrush, and the velocity are 0.1 m/s, 1 m/s, 2 m/s, 3 m/s and 4 m/s, respectively. The left and right tunnel entrances are both the outlets of water inrush, and the pressure is 0 Pa. The pressure here refers to the relative pressure in the Fluent. As shown in Fig. 3, A is the water inrush position. Five case studies of water inrush are simulated and investigated.

3.1 Simulated results and analysis

Under different velocities of water inrush, in order to show the changes of velocity and pressure in the tunnels more clearly, three probing lines are selected respectively in the left tunnel, cross passage, right tunnel and along the height direction of the tunnel centerline. The details of the probing lines are shown in Table 3, and the locations of the probing lines are shown in Fig. 4. The probing lines are researched and analyzed.

3.1.1 The left tunnel

Taking the second probing line N2 (X=-18) in the left tunnel (Fig. 4(a)) as an example, its velocity curves and pressure curves are shown in Fig. 5.

(1) Fig. 5(a) shows that: On the whole, under five velocities of water inrush, the flow velocity of the probing line N2 basically keeps unchanged at their respective water-inrush velocity. Moreover, as the water-inrush velocity increases, the flow velocity of the probing line N2 also increases proportionately. That is to say, when the water-inrush velocity is 0.1 m/s, the flow velocity of the probing line N2 basically keeps unchanged at 0.1 m/s. When the water-inrush velocity is 1 m/s, the flow velocity of the probing line N2 basically keeps unchanged at 1 m/s. When the water-inrush velocity is 2 m/s, the flow velocity of the probing line N2 basically keeps unchanged at 2 m/s. When the water-inrush velocity is 3 m/s, the flow velocity of the probing line N2 basically keeps unchanged at 3 m/s. When the water-inrush velocity is 4 m/s, the flow velocity of the probing line N2 basically keeps unchanged at 4 m/s.

(2) Fig. 5(b) shows that: Overall, the pressure is the maximum at the initial point (Inlet A) of the probing line N2. Then the pressure decreases gradually, and it reduces to 0 Pa at the end point (Outlet 1) of the probing line N2. In addition, under five velocities of water inrush, at the same location of the probing line N2, the pressure change is not proportional to their corresponding change of water-inrush velocity.

3.1.2 The cross passage

Taking the second probing line N5 (Z=50) in the cross passage (Fig. 4(b)) as an example, its velocity curves and pressure curves are shown in Fig. 6.

(1) Fig. 6(a) shows that: The flow velocity is the maximum at the initial point (X=-12) of the probing line N5. Then, the flow velocity reduces sharply when the variation range of X is from -12 to -10, and the flow

velocity changes gently when the variation range of X is from -10 to 12. Overall, the flow velocity has a decreasing trend. In addition, as the water-inrush velocity increases, the flow velocity of the probing line N5 also increases proportionately.

(2) Fig. 6(b) shows that: Under five velocities of water inrush, when the variation range of X is from -12 to -10, the pressure of the probing line N5 decreases gradually,

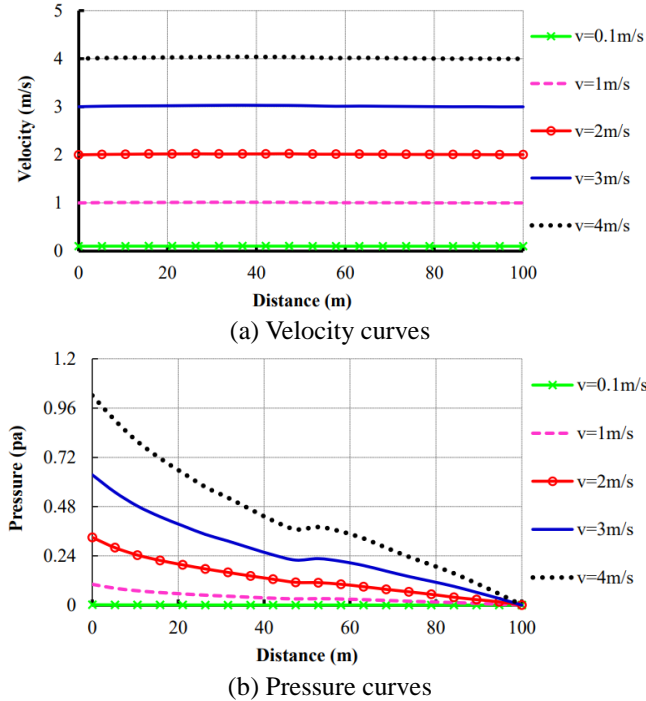


Fig. 5 Velocity and pressure curves of the probing line N2 in the left tunnel

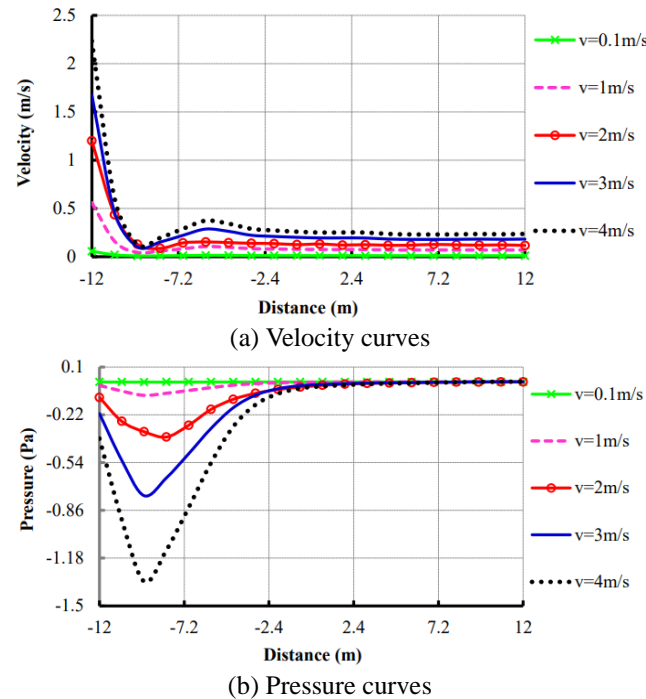


Fig. 6 Velocity and pressure curves of the probing line N5 in the cross passage

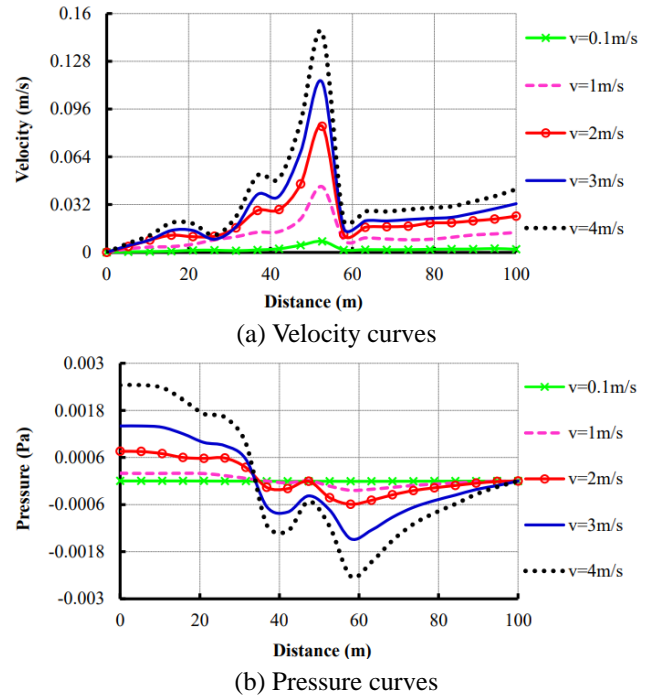


Fig. 7 Velocity and pressure curves of the probing line N8 in the right

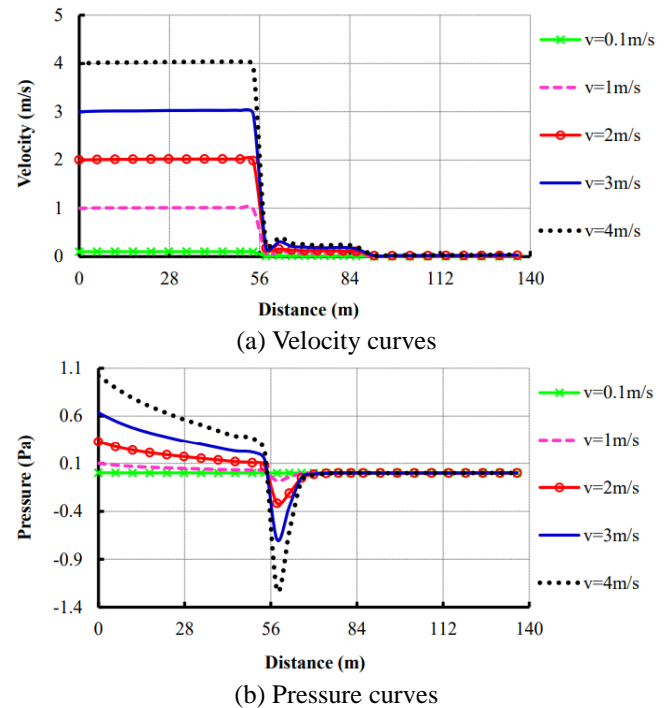


Fig. 8 Velocity and pressure curves of the probing broken line N11

and it reaches its maximum negative pressure when X=-10. When the variation range of X is from -10 to 0, the pressure gradually increases to 0 Pa. When the variation range of X is from 0 to 12, the pressure basically keeps unchanged at 0 Pa. Overall, the pressure decreases firstly and then increases. Moreover, at the same location of the probing line N5, the pressure change is not proportional to their corresponding change of water-inrush velocity.

3.1.3 The right tunnel

Taking the second probing line N8 ($X=18$) in the right tunnel (Fig. 4(c)) as an example, its velocity curves and pressure curves are shown in Fig. 7.

(1) Fig. 7(a) shows that: Under five velocities of water inrush, the flow velocity is 0 m/s at the initial point ($Z=0$) of the probing line N8. When the variation range of Z is from 0 to 52.5, the flow velocity increases gradually, and it reaches its maximum value when $Z=52.6$. Then the flow velocity decreases sharply when the variation range of Z is from 52.6 to 58, while it changes gently when the variation range of Z is from 58 to 100. In short, the flow velocity of the probing line N8 first increases and then decreases. In addition, the flow velocity of the probing line N8 increases with the water-inrush velocity, which has the same increasing linear relationship between them.

(2) Fig. 7(b) shows that: When the velocity of water inrush is 0.1m/s, the pressure of the probing line N8 keeps at 0 Pa unchanged. Under the other four velocities of water inrush, when the variation range of Z is from 0 to 58, the maximum positive pressure gradually reduced to the maximum negative pressure. When the variation range of Z is from 58 to 100, the pressure gradually increases to 0 Pa.

In addition, it also can be concluded, the pressure of the probing line N8 increases with the water-inrush velocity, but it is not a direct linear relationship between them.

3.1.4 The Y-direction

Taking the second probing line N11 ($Y=2$) in the height direction (Y -direction) of the tunnel centerline (Fig. 4(d)) as an example, its velocity curves and pressure curves are shown in Fig. 8.

(1) Fig. 8(a) shows that: Under five velocities of water inrush, the flow velocity of the probing broken line N11 in the left tunnel keeps unchanged at their respective water-inrush velocity. In the process of flowing from the left tunnel to the cross passage, the flow velocity declines sharply, and then it decreases slowly. The flow velocity is close to 0 m/s in the right tunnel. Overall, the flow velocity of the probing broken line N11 reduces with the increase of the distance. In addition, as the velocity of water inrush multiplies, the flow velocity of the probing broken line N11 also multiplies correspondingly.

(2) Fig. 8(b) shows that: In the left tunnel, the pressure decreases gradually. The pressure first decreases and then increases quickly at the intersection area of the left tunnel and the cross passage. Then the pressure changes gently. Overall, the pressure of the probing broken line N10 attains its maximum positive value at the position of the left tunnel working face (Inlet A), and gets its maximum negative value near by the cross passage, besides, the pressure is close to 0 Pa in the right tunnel. In addition, it also can be concluded, the pressure of the probing broken line N10 doesn't increase in proportion with more water-inrush velocity. For example, under five velocities of water inrush, their corresponding pressure curves coincides well in the latter half of the probing broken line N10, showing that the pressure values are basically the same in either case.

3.2 Discussion

As for the selected four groups probing lines in the left

Table 4 Velocity and pressure values of the probing lines (N1, N2 and N3) under each water-inrush velocity

Water-inrush velocity (m/s)	Probing lines	V_{\min} (m/s)	V_{\max} (m/s)	P_{\min} (Pa)	P_{\max} (Pa)
0.1	N1	0.095	0.1	0	0.002
	N2	0.1	0.102	0	0.002
	N3	0.089	0.1	0	0.002
1	N1	0.96	1	0	0.11
	N2	1	1.02	0	0.1
	N3	0.9	1	0	0.11
2	N1	1.92	2	0	0.35
	N2	2	2.02	0	0.33
	N3	1.84	2.01	0	0.35
3	N1	2.88	3	0	0.67
	N2	3	3.03	0	0.64
	N3	2.72	3	0	0.67
4	N1	3.85	4	0	1.07
	N2	4	4.04	0	1.02
	N3	3.64	4.01	0	1.06

Table 5 Velocity and pressure values of the probing lines (N4, N5 and N6) under each water-inrush velocity

Water-inrush velocity (m/s)	Probing lines	V_{\min} (m/s)	V_{\max} (m/s)	P_{\min} (Pa)	P_{\max} (Pa)
0.1	N4	0.002	0.015	-0.001	0
	N5	0.009	0.057	-0.001	0
	N6	0.003	0.024	0	0.001
1	N4	0.013	0.148	-0.094	0
	N5	0.045	0.56	-0.09	0
	N6	0.018	0.243	-0.07	0.08
2	N4	0.014	0.474	-0.395	0
	N5	0.117	1.2	-0.369	0
	N6	0.04	0.335	-0.32	0.271
3	N4	0.034	0.444	-0.789	0.002
	N5	0.101	1.68	-0.762	0
	N6	0.114	0.729	-0.574	0.63
4	N4	0.045	0.592	-1.38	0.003
	N5	0.126	2.23	-1.34	0.001
	N6	0.057	0.973	-1.01	1.08

tunnel, cross passage, right tunnel and in the height direction of the tunnel centerline, the change rules of velocity and pressure for each group probing lines are discussed under the same water-inrush velocity. Finally, water flow characteristics after inrush from the tunnel face are summarized by comparing the case studies.

3.2.1 The left tunnel

In the left tunnel, the range of velocity and pressure for the three probing lines (N1, N2 and N3) under each water-inrush velocity is listed respectively in Table 4.

(1) The flow velocities of the three probing lines have a slight fluctuation on the basis of each water-inrush velocity,

Table 6 Velocity and pressure values of the probing lines (N7, N8 and N9) under each water-inrush velocity

Water-inrush velocity (m/s)	Probing lines	V_{min} (m/s)	V_{max} (m/s)	P_{min} (Pa)	P_{max} (Pa)
0.1	N7	0	0.006	0	0
	N8	0	0.007	0	0
	N9	0	0.006	0	0
1	N7	0	0.033	-0.0002	0.0002
	N8	0	0.044	-0.0002	0.0002
	N9	0	0.034	-0.0001	0.0009
2	N7	0	0.069	-0.0009	0.0008
	N8	0	0.084	-0.0006	0.0008
	N9	0	0.062	-0.0003	0.003
3	N7	0	0.083	-0.0015	0.0014
	N8	0	0.114	-0.0015	0.0014
	N9	0	0.087	-0.0011	0.006
4	N7	0	0.106	-0.0025	0.0025
	N8	0	0.147	-0.0024	0.0024
	N9	0	0.113	-0.0019	0.01

Table 7 Velocity and pressure values of the probing lines (N10, N11 and N12) under each water-inrush velocity

Water-inrush velocity (m/s)	Probing lines	V_{min} (m/s)	V_{max} (m/s)	P_{min} (Pa)	P_{max} (Pa)
0.1	N10	0	0.035	0	0.002
	N11	0.002	0.102	0	0.002
	N12	0	0.104	0	0.002
1	N10	0.003	0.353	-0.079	0.108
	N11	0.009	1.01	-0.082	0.101
	N12	0.003	1.03	-0.074	0.096
2	N10	0.006	0.704	-0.346	0.348
	N11	0.015	2.02	-0.315	0.33
	N12	0.004	2.04	-0.312	0.317
3	N10	0.006	1.06	-0.665	0.66
	N11	0.02	3.03	-0.693	0.635
	N12	0.006	3.06	-0.626	0.613
4	N10	0.007	1.41	-1.17	1.06
	N11	0.026	4.04	-1.22	1.02
	N12	0.008	4.07	-1.1	0.992

and the variation range of flow velocity is little. Moreover, as for the three probing lines N1 ($X=-14$), N2 ($X=-18$) and N3 ($X=-22$) under each water-inrush velocity, the flow velocity in the center of the section is the maximum, and then it decreases gradually toward both sides of the section, i.e., the flow velocity of the probing line N2 is the maximum, while the velocities of the probing lines N1 and N3 are relatively small.

(2) The pressure changes of the three probing lines N1, N2 and N3 are basically the same under each water-inrush velocity, which shows that the pressure values along the length direction (Z -direction) of the left tunnel are basically fixed in Y section of the left tunnel.

3.2.2 The cross passage

In the cross passage, the range of velocity and pressure for the three probing lines (N4, N5 and N6) under each water-inrush velocity is listed respectively in Table 5.

(1) Compared with the left tunnel, the flow velocities of the three probing lines in the cross passage are obviously reduced, especially at the beginning of the probing lines, the flow velocity declines sharply. Moreover, for the selected three probing lines N4 ($Z=48.4$), N5 ($Z=50$) and N6 ($Z=51.6$), the flow velocity in the center of the section is the maximum, and then it decreases gradually toward both sides of the section, i.e., the flow velocity of the probing line N5 is the maximum, while the velocities of the probing lines N4 and N6 are relatively small.

(2) Under each water-inrush velocity, the pressure changes greatly on the starting location of the cross passage. Specifically the pressure changes of the probing lines N4 and N5 are basically the same, and compared with the first two probing lines, the pressure change of the probing line N6 is relatively larger. While in the mid-posterior segment of the cross passage, the pressure changes of the three probing lines are in good agreement.

3.2.3 The right tunnel

In the right tunnel, the range of velocity and pressure for the three probing lines (N7, N8 and N9) under each water-inrush velocity is listed respectively in Table 6.

(1) Compared with the cross passage, the flow velocities of the three probing lines in the right tunnel are obviously reduced, and they all change greatly near by the cross passage. In addition, for the corresponding three probing lines N7 ($X=14$), N8 ($X=18$) and N9 ($X=22$) under each water-inrush velocity, the flow velocity in the center of the section is the maximum, and then it decreases gradually toward both sides of the section, i.e., the flow velocity of the probing line N8 is the maximum, while the flow velocities of the probing lines N7 and N9 are relatively small.

(2) Compared with the left tunnel and the cross passage, the pressure in the right tunnel is very little, which is close to 0 Pa. To be specific, the pressure changes of the probing lines N7 and N8 are basically the same, and compared with the first two probing lines, the pressure variation of the probing line N9 is relatively larger, especially in the vicinity of the cross passage.

3.2.4 The Y -direction

In the Y -direction, the range of velocity and pressure for the three probing lines (N10, N11 and N12) under each water-inrush velocity is listed respectively in Table 7.

(1) It can be concluded that, in the left tunnel, the flow velocity increases with the Y , i.e., the flow velocity of the probing broken line N10 ($Y=0.4$) is the minimum, and the flow velocity of the probing broken line N12 ($Y=3.6$) is the maximum. In the cross passage, the flow velocity in the center of the section is the maximum, and then it gradually decreases toward the upper and lower, i.e., the flow velocity of the probing broken line N11 ($Y=2$) is the maximum, while the flow velocities of the probing broken lines N10 ($Y=0.4$) and N12 ($Y=3.6$) are relatively small. In the right tunnel, the flow velocities of the three probing broken lines are all very small no matter what velocity of water inrush it

is, and their corresponding velocity curves are in good agreement. Overall, the flow velocity decreases gradually with the increase of distance, and it is close to 0 m/s in the right tunnel.

(2) The pressure changes of the three probing broken lines N10, N11 and N12 are in good agreement, which shows that the pressure values along the length direction of the tunnel are basically fixed in the height direction (Y-direction) of the tunnel. Overall, the pressure decreases gradually with the increase of distance, and it is close to 0 Pa in the right tunnel.

3.2.5 General description

(1) Under five velocities of water inrush, the changes of flow velocity have obvious differences in the left tunnel, but the variation difference is very small in the cross passage and the right tunnel. This shows that, starting from the water inrush position (Inlet A), the water flows to outside (Outlet 1) mainly through the left tunnel.

(2) Under five velocities of water inrush, the changes of pressure have obvious differences in the left tunnel and the cross passage, or rather, the pressure changes greatly at the intersection area of the cross passage and the left tunnel. But the changes of pressure are very little in the right tunnel, which value retains at around 0 Pa.

(3) Under each water-inrush velocity, as for the corresponding multi-group probing lines, the flow velocity is the maximum in the center of the section, while it is the minimum at boundaries.

(4) Under each water-inrush velocity, according to the pressure changes of the multi-group probing lines, it can be concluded that the pressure value of every cross section in the tunnels is basically fixed.

(5) As the water-inrush velocity increases, the flow velocity in the tunnels also increases proportionately.

(6) The pressure in the tunnels increases with the water-inrush velocity, but there exists no direct linear relationship between them.

4. The second class case studies

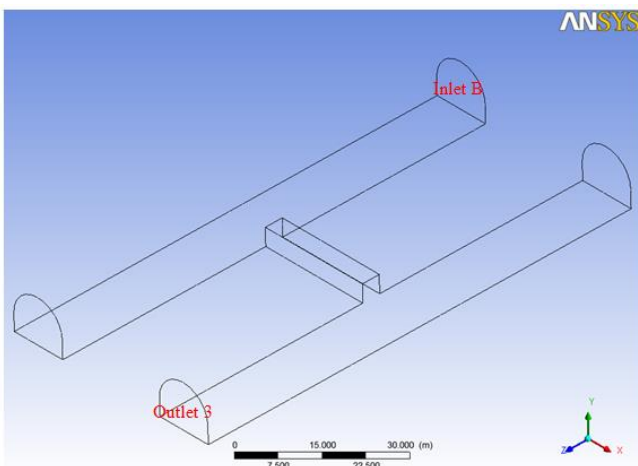
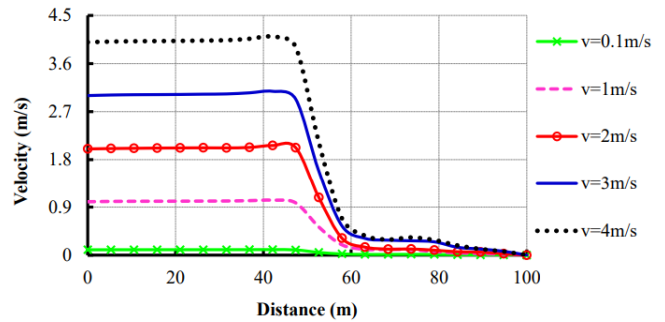
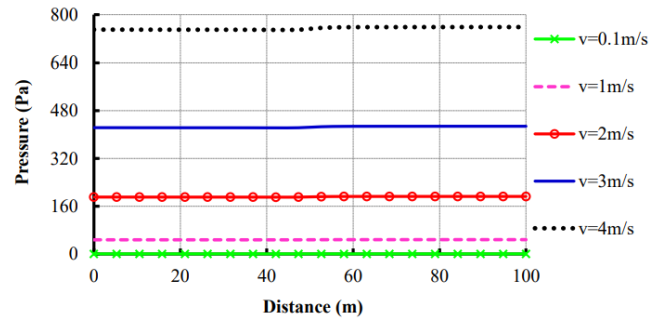


Fig. 9 The water inrush conditions during the double-line tunnel excavation



(a) Velocity curves



(b) Pressure curves

Fig. 10 Velocity and pressure curves of the probing line N2 in the left tunnel

The following case may be encountered during the double-line tunnel excavation. In the process of the left tunnel excavation, the tunneling cannot be carried out due to the effects of geological conditions and other factors. At this time, the right tunnel should first be excavated, and then both ends of the left tunnel are further excavated after passing through the cross passage.

Then during the left tunnel excavation, water inrush occurs on the left tunnel working face (away from the left tunnel entrance), thus, the left tunnel working face is the inlet of water inrush, and the velocity are 0.1 m/s, 1 m/s, 2 m/s, 3 m/s and 4 m/s, respectively. Only the right tunnel entrance is the outlet of water inrush, and the pressure is 0 Pa. As shown in Fig. 9, B is the water inrush position. Five case studies of water inrush are simulated and investigated.

4.1 Simulated results and analysis

Under different velocities of water inrush, in order to show the changes of velocity and pressure in the tunnels more clearly, three probing lines are selected respectively in the left tunnel, cross passage, right tunnel and along the height direction of the tunnel centerline. The selection of the probing lines is the same as the first class case studies. The details of the probing lines are shown in Table 3, and the locations of the probing lines are shown in Fig. 4. The probing lines are researched and analyzed.

4.1.1 The left tunnel

Taking the second probing line N2 (X=-18) in the left tunnel (Fig. 4(a)) as an example, its velocity curves and pressure curves are shown in Fig. 10.

(1) Fig. 10(a) shows that: Under five velocities of water inrush, in the first half of the probing line N2, the flow

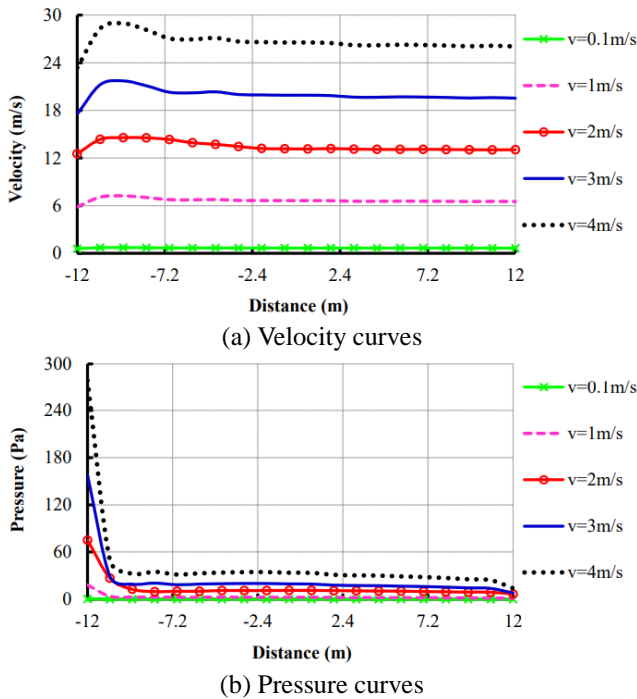


Fig. 11 Velocity and pressure curves of the probing line N5 in the cross passage

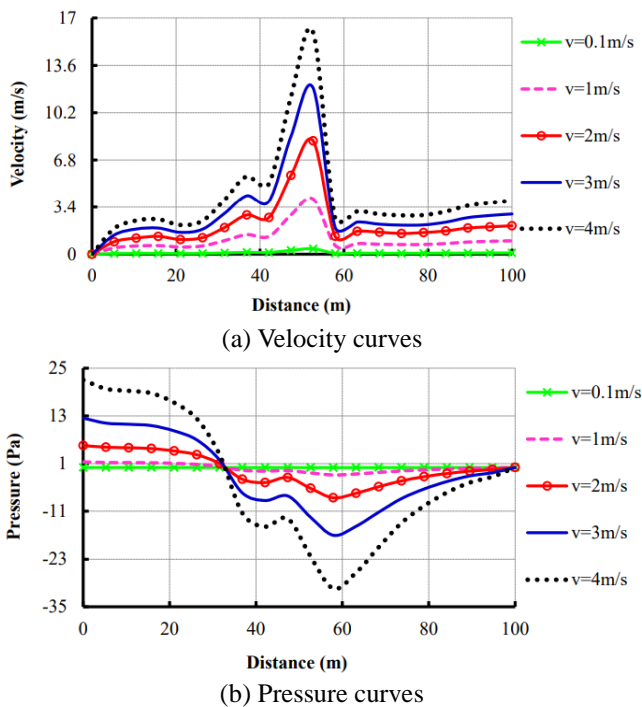


Fig. 12 Velocity and pressure curves of the probing line N8 in the right tunnel

velocity is approximately equal to their respective water-inrush velocity. The flow velocity declines rapidly in the vicinity of the cross passage, and then it decreases slowly. The flow velocity reduces to 0 m/s at the end point of the probing line N2. Overall, the flow velocity of the probing line N2 shows a downward trend. Besides, the flow velocity of the probing line N2 rises in proportion with more water-inrush velocity.

(2) Fig. 10(b) shows that: On the whole, the pressure of the probing line N2 changes more gently, moreover, under five velocities of water inrush, as the water-inrush velocity increases, the pressure of the probing line N2 also increases, but there exists no direct linear relationship between them.

4.1.2 The cross passage

Taking the second probing line N5 ($Z=50$) in the cross passage (Fig. 4(b)) as an example, its velocity curves and pressure curves are shown in Fig. 11.

(1) Fig. 11(a) shows that: On the whole, the flow velocity first increases and then decreases in the former half of the probing line N5, and it changes more gently in the latter half of the probing line N5. Moreover, under five velocities of water inrush, as the water-inrush velocity increases, the flow velocity of the probing line N5 also increases proportionately.

(2) Fig. 11(b) shows that: Overall, the pressure of the probing line N5 has a decreasing trend, and it declines more obviously at the initial point of the probing line N5. In addition, under five velocities of water inrush, at the same location of the probing line N5, the pressure change is not proportional to their corresponding change of water-inrush velocity.

4.1.3 The right tunnel

Taking the second probing line N8 ($X=18$) in the right tunnel (Fig. 4(c)) as an example, its velocity curves and pressure curves are shown in Fig. 12.

(1) Fig. 12(a) shows that: Under five velocities of water inrush, the flow velocity is 0 m/s at the initial point of the probing line N8. Then the flow velocity gradually increases with the distance, and it reaches its maximum value at the intersection area of the cross passage and the right tunnel. Later the flow velocity declines sharply, while it changes gently in the latter half of the probing line N8. In addition, it also can be concluded that the flow velocity of the probing line N8 increases in proportion with more water-inrush velocity.

(2) Fig. 12(b) shows that: On the whole, the pressure is the maximum at the starting point of the probing line N8, and then it decreases gradually. The pressure reaches its maximum negative value when $Z=58$, later the pressure gradually increases, and it becomes to 0 Pa at the end point of the probing line N8. Besides, under five velocities of water inrush, at the same location of the probing line N8, the pressure change is not proportional to their corresponding change of water-inrush velocity.

4.1.4 The Y-direction

Taking the second probing line N11 ($Y=2$) in the height direction (Y-direction) of the tunnel centerline (Fig. 4(d)) as an example, its velocity curves and pressure curves are shown in Fig. 13.

(1) Fig. 13(a) shows that: Under five velocities of water inrush, the flow velocity of the probing broken line N11 in the left tunnel keeps unchanged at their respective water-inrush velocity. In the process of flowing from the left tunnel to the cross passage, the flow velocity increases quickly, and then it decreases slowly. In the process of flowing from the cross passage to the right tunnel, the flow

velocity declines sharply, and then it changes gently. Overall, the flow velocity of the probing broken line N11 changes greatly at the intersection area of the cross passage and the tunnels, while it changes gently in other areas. In addition, it also can be concluded that the flow velocity of the probing broken line N11 rises in proportion with more water-inrush velocity.

(2) Fig. 13(b) shows that: In the left tunnel, the pressure of the probing broken line N10 basically keeps unchanged, and it declines sharply at the intersection area of the left tunnel and the cross passage. Overall, the pressure change of the probing broken line N10 is the maximum at the intersection area of the left tunnel and the cross passage, while it is relatively small in other areas. In addition, it also can be concluded, under five velocities of water inrush, as the water-inrush velocity increases, the pressure of the probing broken line N10 also increases, but there exists no direct linear relationship between them.

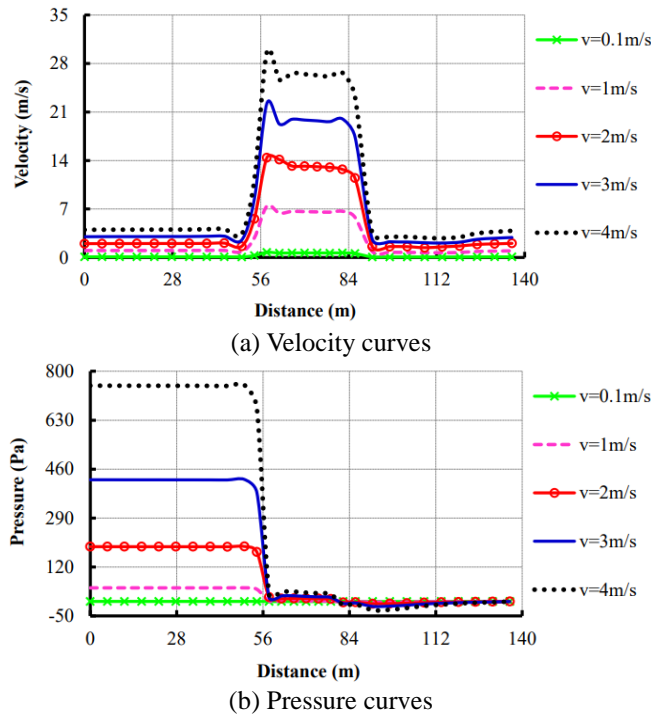


Fig. 13 Velocity and pressure curves of the probing broken line N11

Table 8 Velocity and pressure values of the probing lines (N1, N2 and N3) under each water-inrush velocity

Water-inrush velocity (m/s)	Probing lines	V_{min} (m/s)	V_{max} (m/s)	P_{min} (Pa)	P_{max} (Pa)
0.1	N1	0	0.224	0.469	0.49
	N2	0	0.103	0.484	0.49
	N3	0	0.1	0.485	0.49
1	N1	0	2.24	46	48
	N2	0	1.03	47.5	48
	N3	0	1	47.5	48
2	N1	0	4.87	175	193
	N2	0	2.06	190	193
	N3	0	2.01	191	193

Table 8 Continued

Water-inrush velocity (m/s)	Probing lines	V_{min} (m/s)	V_{max} (m/s)	P_{min} (Pa)	P_{max} (Pa)
3	N1	0	6.71	397	428
	N2	0	3.08	423	428
	N3	0	3	423	428
4	N1	0	8.94	704	759
	N2	0	4.1	749	759
	N3	0	4.01	750	759

Table 9 Velocity and pressure values of the probing lines (N4, N5 and N6) under each water-inrush velocity

Water-inrush velocity (m/s)	Probing lines	V_{min} (m/s)	V_{max} (m/s)	P_{min} (Pa)	P_{max} (Pa)
0.1	N4	0.002	0.015	-0.035	0.14
	N5	0.136	0.266	0.01	0.188
	N6	0.585	0.723	-0.003	0.2
1	N4	1.36	2.66	-4.32	13.1
	N5	5.85	7.23	0.919	18
	N6	1.55	3.25	-1.29	19
2	N4	3.44	4.95	-26	52.3
	N5	12.5	14.6	6.52	75.1
	N6	3.43	4.92	0.382	74.3
3	N4	4.08	7.97	-42.5	113
	N5	17.5	21.7	7.92	158
	N6	4.66	9.77	-16.5	165
4	N4	5.44	10.6	-77.2	199
	N5	23.4	29	13.9	279
	N6	6.21	13	-31.6	291

4.2 Discussion

As for the selected four groups probing lines in the left tunnel, cross passage, right tunnel and in the height direction of the tunnel centerline, the change rules of velocity and pressure for each group probing lines under the same water-inrush velocity are discussed. Finally, water flow characteristics after inrush from the tunnel face are summarized by comparing the case studies.

4.2.1 The left tunnel

In the left tunnel, the range of velocity and pressure for the three probing lines (N1, N2 and N3) under each water-inrush velocity is listed respectively in Table 8.

(1) Under each water-inrush velocity, the flow velocities of the three probing lines N1 ($X=-14$), N2 ($X=-18$) and N3 ($X=-22$) all change greatly near by the cross passage, moreover, the flow velocity closing to the side of cross passage is the maximum, and then it gradually decreases toward the other side, i.e., the flow velocity of the probing line N1 is the maximum, while the flow velocity of the probing lines N3 is the minimum. In other areas of the left tunnel, the flow velocity changes of the three probing lines are basically the same.

(2) Under each water-inrush velocity, the pressures of

the three probing lines N1 ($X=-14$), N2 ($X=-18$) and N3 ($X=-22$) all change greatly in the vicinity of the cross passage, moreover, the pressure change closing to the side of cross passage is the maximum, and then it gradually decreases toward the other side, i.e., the pressure change of the probing line N1 is the maximum, while the probing lines N3's is the minimum. In other areas of the left tunnel, the pressure changes of the three probing lines are basically the same.

4.2.2 The cross passage

In the cross passage, the range of velocity and pressure for the three probing lines (N4, N5 and N6) under each water-inrush velocity is listed respectively in Table 9.

(1) It can be seen that, compared with the left tunnel, the flow velocities of the three probing lines in the cross passage are obviously increased. Moreover, under each water-inrush velocity, for the selected three probing lines N4 ($Z=48.4$), N5 ($Z=50$) and N6 ($Z=51.6$), the flow velocity in the center of the section is the maximum, and then it decreases gradually toward both sides of the section, i.e., the flow velocity of the probing line N5 is the maximum, while the velocities of the probing lines N4 and N6 are relatively small.

(2) It can be concludes that, under each water-inrush velocity, the pressure changes of the three probing lines N4, N5 and N6 are all large on the starting location of the cross passage, while the pressure changes are in good agreement in other areas of the cross passage.

4.2.3 The right tunnel

In the right tunnel, the range of velocity and pressure for the three probing lines (N7, N8 and N9) under each water-inrush velocity is listed respectively in Table 10.

(1) Under each water-inrush velocity, the flow velocities of the three probing lines all change greatly in the vicinity of the cross passage. In the former half of the right tunnel, for the selected three probing lines N7 ($X=14$), N8 ($X=18$) and N9 ($X=22$), the flow velocity in the center of the section is the maximum, and then it decreases gradually toward both sides of the section, i.e., the flow velocity of the probing line N8 is the maximum, while the flow velocities of the probing lines N7 and N9 are relatively small. In the latter half of the right tunnel, the velocity closing to the side of cross passage is the maximum, and then it gradually decreases toward the other side, i.e., the flow velocity of the probing line N7 is the maximum, while the flow velocity of the probing line N9 is the minimum.

(2) Compared with the left tunnel and the cross passage, the pressures of the probing lines in the right tunnel are obviously reduced. Under each water-inrush velocity, the pressure of each probing line changes greatly near by the cross passage, moreover, for the selected three probing lines N7 ($X=14$), N8 ($X=18$) and N9 ($X=22$), the pressure change of the probing line N9 is the maximum.

4.2.4 The Y-direction

In the Y-direction, the range of velocity and pressure for the three probing lines (N10, N11 and N12) under each water-inrush velocity is listed respectively in Table 11.

(1) Under each water-inrush velocity, in the left tunnel,

Table 10 Velocity and pressure values of the probing lines (N7, N8 and N9) under each water-inrush velocity

Water-inrush velocity (m/s)	Probing lines	V_{\min} (m/s)	V_{\max} (m/s)	P_{\min} (Pa)	P_{\max} (Pa)
0.1	N7	0	0.296	-0.021	0.015
	N8	0	0.397	-0.018	0.014
	N9	0	0.323	-0.012	0.074
1	N7	0	2.97	-2.19	1.45
	N8	0	3.99	-1.88	1.4
	N9	0	3.24	-1.2	7.4
2	N7	0	6.38	-9.64	5.83
	N8	0	8.19	-7.63	5.53
	N9	0	6.33	-4.35	30.7
3	N7	0	8.93	-20	13
	N8	0	12	-17.1	12.4
	N9	0	9.73	-10.9	66.5
4	N7	0	11.9	-35.6	23
	N8	0	16	-30.4	22.1
	N9	0	13	-19.4	118

Table 11 Velocity and pressure values of the probing lines (N10, N11 and N12) under each water-inrush velocity

Water-inrush velocity (m/s)	Probing lines	V_{\min} (m/s)	V_{\max} (m/s)	P_{\min} (Pa)	P_{\max} (Pa)
0.1	N10	0.022	0.257	-0.017	0.486
	N11	0.069	0.74	-0.018	0.486
	N12	0.02	0.51	-0.02	0.487
1	N10	0.228	2.57	-1.7	47.7
	N11	0.692	7.4	-1.85	47.6
	N12	0.186	5.08	-2.13	47.7
2	N10	0.523	6.37	-6.92	191
	N11	1.42	14.4	-7.6	191
	N12	0.325	9.16	-10.4	191
3	N10	0.69	7.72	-15.5	424
	N11	2.09	22.2	-16.8	424
	N12	0.548	15.2	-19.3	423
4	N10	0.921	10.3	-27.6	752
	N11	2.78	29.6	-30	750
	N12	0.727	20.3	-34.5	750

the flow velocity increases with the Y, i.e., the flow velocity of the probing broken line N10 ($Y=0.4$) is the minimum, and the flow velocity of the probing broken line N12 ($Y=3.6$) is the maximum. In the cross passage, the flow velocity in the center of the section is the maximum, and then it gradually decreases toward the upper and lower, i.e., the flow velocity of the probing broken line N11 ($Y=2$) is the maximum, while the flow velocities of the probing broken lines N10 ($Y=0.4$) and N12 ($Y=3.6$) are relatively small. In the right tunnel, the flow velocity in the center of the section is the maximum, and then it gradually decreases toward the upper and lower, i.e., the flow velocity of the probing broken line N11 is the maximum, while the flow

velocities of the probing broken lines N10 and N12 are relatively small.

(2) Under each water-inrush velocity, the pressure of each probing broken line is the maximum in the left tunnel, flowed by the cross passage, and it is the minimum in the right tunnel. Moreover, the pressure curves of the three probing broken lines N10, N11 and N12 coincide well, which shows that the pressure values along the length direction of the tunnel are basically fixed in the height direction (Y-direction) of the tunnel.

4.2.5 General description

(1) Under five velocities of water inrush, the flow velocity is large in the cross passage, while it is relatively small in the left and right tunnels. The flow velocity change is the maximum at the intersection area of the cross passage and the tunnels, which has obvious differences. This shows that, starting from the water inrush position (Inlet B), the water mainly flows to the cross passage, and then turns to the right tunnel entrance (Outlet 3).

(2) Under five velocities of water inrush, the pressure is the maximum in the left tunnel, flowed by the cross passage, and it is the minimum in the right tunnel. Moreover, the pressure changes greatly at the intersection area of the cross passage and the tunnels.

(3) Under each water-inrush velocity, as for the corresponding multi-group probing lines, in most cases, the flow velocity is the maximum in the center of the section, while it is the minimum at boundaries.

(4) Under each water-inrush velocity, according to the pressure changes of the multi-group probing lines, it can be concluded, except for the intersection area of the cross passage and the tunnels, the pressure value of every cross section in the tunnels is basically fixed.

(5) The flow velocity in the tunnels increases with the water-inrush velocity, and both of them have the same increasing linear relationship.

(6) The pressure in the tunnels increases with the water-inrush velocity, but there exists no direct linear relationship between them.

5. Conclusions

Flow characteristics after water inrush from the working face in karst tunneling are investigated in the present study. Numerical calculation for two class case studies of water inrush is carried out by using the FLUENT software. For each class water inrush from the tunnel face, five cases under different water-inrush velocities are simulated and researched. The variation characteristics of velocity and pressure on each probing line under the five water-inrush velocities are analyzed. The change rules of velocity and pressure on each group probing lines under one water-inrush velocity are discussed. Finally, the water flow characteristics after inrush from the tunnel face are summarized by comparing these case studies, and the following conclusions are drawn:

(1) The velocity and pressure change greatly at the intersection area of the cross passage and the tunnels.

(2) In general, the velocity nearby the tunnel side wall is

the minimum, while it is the maximum in the middle position.

(3) The pressure value of every cross section in the tunnels is basically fixed except for the intersection area of the cross passage and the tunnels.

(4) The flow velocity in the tunnels increases with the water-inrush velocity, and both of them have a same increasing linear relationship.

(5) The pressure in the tunnels increases with the water-inrush velocity, but it is not a direct linear relationship between them.

Acknowledgements

The research was financially supported by the National Natural Science Foundation of China (Grant No.: 51509147) and the National Basic Research Program of China (973 Program, Grant No.: 2013CB036000).

References

- Chen, L.W., Zhang, S.L. and Gui, H.R. (2014), "Prevention of water and quicksand inrush during extracting contiguous coal seams under the lowermost aquifer in the unconsolidated Cenozoic alluvium-a case study", *Arab. J. Geosci.*, **7**(6), 2139-2149.
- Divall, S. and Goodey, R.J. (2015), "Twin-tunnelling-induced ground movements in clay", *Proc. Inst. Civ. Eng. Geotech.*, **168**(3), 247-256.
- Fahimifar, A., Ghadami, H. and Ahmadvand, M. (2015), "The ground response curve of underwater tunnels, excavated in a strain-softening rock mass", *Geomech. Eng.*, **8**(3), 323-359.
- Georgiannou, V.N., Lefas, I.D. and Boronkay, K.A. (2006), "Monitoring of tunnel behaviour through cataclastic rocks", *Proc. Inst. Civ. Eng. Geotech.*, **159**(2), 113-123.
- Golob, R., Stokelj, T. and Grgic, D. (1998), "Neural-network-based water inflow forecasting", *Control Eng. Pract.*, **6**(5), 593-600.
- Hu, Y., Yan, G. and Shi, X. (2008), "Study on physical and numerical simulation of water inrush prediction theory for coal mining above confined aquifer", *Chin. J. Rock Mech. Eng.*, **27**(1), 9-15.
- Huang, C.H., Feng, T., Wang, W.J. and Liu, H. (2010), "Mine water inrush prediction based on fractal and support vector machines", *J. Chin. Coal Soc.*, **35**(5), 806-810.
- Islam, M.R. and Islam, M.S. (2005), "Water inrush hazard in Barapukuria coal mine, Dinajpur District, Bangladesh", *Bangl. J. Geol.*, **24**(1), 1-17.
- Ivars, D.M. (2006), "Water inflow into excavations in fractured rock-a three-dimensional hydro-mechanical numerical study", *J. Rock Mech. Min. Sci.*, **43**(5), 705-725.
- Jiang, F.X., Ye, G.X., Wang, C.W., Zhang, D.Y. and Guan, Y.Q. (2008), "Application of high-precision microseismic monitoring technique to water inrush monitoring in coal mine", *Chin. J. Rock Mech. Eng.*, **27**(9), 1932-1938.
- Jin, H., Shi, L.Q., Yu, X.G., Wei, J.C. and Li, S.C. (2009), "Mechanism of mine water-inrush through a fault from the floor", *Min. Sci. Tech.*, **19**(3), 276-281.
- Khezri, N., Mohamad, H. and Fatahi, B. (2016), "Stability assessment of tunnel face in a layered soil using upper bound theorem of limit analysis", *Geomech. Eng.*, **11**(4), 471-492.
- Kong, H.L., Miao, X.X., Wang, L.Z., Zhang, Y. and Chen, Z.Q. (2007), "Analysis of the harmfulness of water-inrush from coal

- seam floor based on seepage instability theory”, *J. China Univ. Min. Tech.*, **17**(4), 453-458.
- Li, L.J., Qian, M.G. and Li, S.G. (1996), “Mechanism of water-inrush through fault”, *J. Chin. Coal Soc.*, **21**(2), 119-123.
- Li, L.P., Li, S.C. and Zhang, Q.S. (2010), “Study of mechanism of water inrush induced by hydraulic fracturing in karst tunnels”, *Rock Soil Mech.*, **31**(2), 523-528.
- Li, S.C., Wu, J., Xu, Z.H., Li, L.P., Huang, X., Xue, Y.G. and Wang, Z.C. (2016), “Numerical analysis of water flow characteristics after inrushing from the tunnel floor in process of karst tunnel excavation”, *Geomech. Eng.*, **10**(4), 471-526.
- Li, X.P. and Li, Y.N. (2014), “Research on risk assessment system for water inrush in the karst tunnel construction based on GIS: case study on the diversion tunnel groups of the Jinping II hydropower station”, *Tunn. Undergr. Sp. Tech.*, **40**, 182-191.
- Ma, L., Liu, Y. and Zhou, X.P. (2010), “Fuzzy comprehensive evaluation method of F statistics weighting in identifying mine water inrush source”, *J. Eng. Sci. Tech.*, **2**(7), 123-128.
- Marinelli, F. and Niccoli, W.L. (2000), “Simple analytical equations for estimating ground water inflow to a mine pit”, *Groundwater*, **38**(2), 311-314.
- Meng, Z.P., Li, G.Q. and Xie, X.T. (2012), “A geological assessment method of floor water inrush risk and its application”, *Eng. Geol.*, **143**, 51-60.
- Nawel, B. and Salah, M. (2015). “Numerical modeling of two parallel tunnels interaction using three-dimensional Finite Elements Method”, *Geomech. Eng.*, **9**(6), 775-791.
- Rao, J.Y., Xie, T. and Liu, Y.M. (2016), “Fuzzy evaluation model for in-service karst highway tunnel structural safety”, *KSCE J. Civ. Eng.*, **20**(4), 1242-1249.
- Shi, L.Q., Qiu, M., Wei, W.X., Xu, D.J. and Han, J. (2014), “Water inrush evaluation of coal seam floor by integrating the water inrush coefficient and the information of water abundance”, *J. Min. Sci. Tech.*, **24**(5), 677-681.
- Tang, J.H., Bai, H.B., Yao, B.H. and Wu, Y. (2011), “Theoretical analysis on water-inrush mechanism of concealed collapse pillars in floor”, *Min. Sci. Tech.*, **21**(1), 57-60.
- Wang, J.H. and Lu, C.C. (2007), “A semi-analytical method for analyzing the tunnel water inflow”, *Tunn. Undergr. Sp. Tech.*, **22**(1), 39-46.
- Wang, J.T. and Wang, X.L. (2011), “Discussion on water inrush coefficient method applied to predict water inrush danger of seam floor based on Gaojiata mine as example”, *Coal Sci. Tech.*, **39**(7), 106-111.
- Wang, Y., Yang, W.F., Li, M. and Liu, X., (2012), “Risk assessment of floor water inrush in coal mines based on secondary fuzzy comprehensive evaluation”, *J. Rock Mech. Min. Sci.*, **52**, 50-55.
- Wei, J.C., Li, Z.J., Shi, L.Q., Guan, Y.Z. and Yin, H.Y. (2010), “Comprehensive evaluation of water-inrush risk from coal floors”, *Min. Sci. Tech.*, **20**(1), 121-125.
- Yang, X.L., Xu, J.S., Li, Y.X. and Yan, R.M. (2016). “Collapse mechanism of tunnel roof considering joined influences of nonlinearity and non-associated flow rule”, *Geomech. Eng.*, **10**(1), 21-35.
- Yao, B.H., Bai, H.B. and Zhang, B.Y. (2012), “Numerical simulation on the risk of roof water inrush in Wuyang Coal Mine”, *J. Min. Sci. Tech.*, **22**(2), 273-277.
- Zarei, H.R., Uromeily, A. and Sharifzadeh, M. (2012), “Identifying geological hazards related to tunneling in carbonate karstic rocks-Zagros, Iran”, *Arab. J. Geosci.*, **5**(3), 457-464.
- Zhang, J.C. (2005), “Investigations of water inrushes from aquifers under coal seams”, *J. Rock Mech. Min. Sci.*, **42**(3), 350-360.
- Zhang, Y.X., Tu, S.H., Bai, Q.S. and Li, J.J. (2013), “Overburden fracture evolution laws and water-controlling technologies in mining very thick coal seam under water-rich roof”, *J. Min. Sci. Tech.*, **23**(5), 693-700.
- Zhou, Z.Q., Li, S.C., Li, L.P., Shi, S.S. and Xu, Z.H. (2015), “An optimal classification method for risk assessment of water inrush in karst tunnels based on the grey system”, *Geomech. Eng.*, **8**(5), 631-647.
- Zhu, Q.H., Feng, M.M. and Mao, X.B. (2008), “Numerical analysis of water inrush from working-face floor during mining”, *J. Chin. Univ. Min. Tech.*, **18**(2), 159-163.

JS